



NIMFEIA

Deliverable D2.2

Report on the available reservoir building blocks

Project Number	101070290
Project name	Nonlinear Magnons for Reservoir Computing in Reciprocal Space
Project acronym	NIMFEIA
Work Package	WP2 Laboratory-scale experiments
Type	Report
Dissemination level	Public
Lead Beneficiary	HZDR
Due date of delivery	Month 30 – March 2025
Author(s)	Katrin Schultheiss (HZDR), Christopher Heins (HZDR), Helmut Schultheiss (HZDR)

Disclaimer:

The NIMFEIA project has received funding by the European Union's Research and Innovation Programme Horizon Europe under grant agreement No 101070290. However, views and opinions expressed in this document are those of the authors only and do not necessarily reflect those of the European Union. The European Union cannot be held responsible for them.

1. Introduction

In the NIMFEIA project, we study alternative solutions for information processing tasks by exploiting the dynamics in the modal space of a magnetic element. This scheme relies on magnon interactions in magnetic materials whereby inputs and outputs correspond to particular eigenmodes of a micromagnetic state. Micrometer-sized magnetic structures can exhibit hundreds of eigenmodes with frequencies in the GHz range¹. Processes such as three magnon-scattering interconnect these modes with each other and, with that, provide the nonlinearity and recurrence required for computing. We refer to this approach as modal multiplexing with signals evolving in reciprocal space, in which the actual computation is performed. This is distinct from other wave-based schemes where information is processed with wave propagation and interference in real space and differs from temporal multiplexing where virtual nodes are constructed with delayed feedback.

With the magnon-scattering reservoir², which we introduced in Deliverable 2.1, we demonstrated the possibility of performing reservoir computing tasks in modal space utilizing the intrinsic nonlinear properties of a magnetic system. Temporal patterns encoded using two different input-frequency pulses were distinguished with high accuracy. This first proof of concept device relied on disk-shaped ferromagnetic microstructures which are magnetized in the vortex state. However, the reservoir shape directly influences the spin structure and the internal magnetic field landscape and, thus, changes the mode distribution in reciprocal space and the nonlinear scattering channels as well. Therefore, it is our goal to extend the operation capacities by combining reservoirs of different shapes, especially, after demonstrating in Deliverable D2.4 that the combination of several vortex-state disks on a single continuous coplanar waveguide antenna does not impede the performance of each individual reservoir.

2. Vortex-based reservoirs with varying diameter and thickness

One feature of the vortex-based magnon reservoir is its operation in reciprocal space exploiting the nonlinear interaction of different quantized eigenmodes. Counterintuitively, this implies that reaching higher node densities requires to pattern larger structures instead of smaller ones. Increasing the reservoir's dimension results in a denser eigenmode spectrum which increases the number of states that are available for nonlinear three-magnon scattering, as is schematically shown by the dispersion relations sketched for disks with different diameter in Fig. 1a-c. Therefore, we patterned a 50 nm-thick Ni₈₁Fe₁₉ film into disk-shaped reservoirs with diameters reaching from 1 μm to 10 μm, as shown in the scanning electron micrographs in Fig. 1d,e. Using Brillouin light scattering (BLS) microscopy, we measure magnon spectra on the different disks, for each integrating over several measurement positions to capture modes with different spatial profiles. The results in Fig. 1f-k demonstrate that nonlinear three-magnon splitting, which is visible in the off-diagonal signals, becomes more pronounced the larger the disk is. In the 1 μm-wide disk (Fig. 1f), only a weak signal from three-magnon scattering is visible around the excitation frequency of 10 GHz, whereas in the 10 μm-wide disk (Fig. 1k), three-magnon splitting is measured over a much wider range of excitation frequencies from 5 GHz to 10 GHz.

Similarly, the density of states can be enhanced by increasing the disks' thickness. In Fig. 2, we compare the magnon BLS spectra recorded for 5 μm-wide Ni₈₁Fe₁₉ disks with thicknesses of 50 nm,

¹ Schultheiss, K. et al. Excitation of whispering gallery magnons in a magnetic vortex. *Phys. Rev. Lett.* 122, 097, 202 (2019).

² Körber, L. et al. Pattern recognition in reciprocal space with a magnon-scattering reservoir. *Nature Comm.* 14, 3954 (2023).



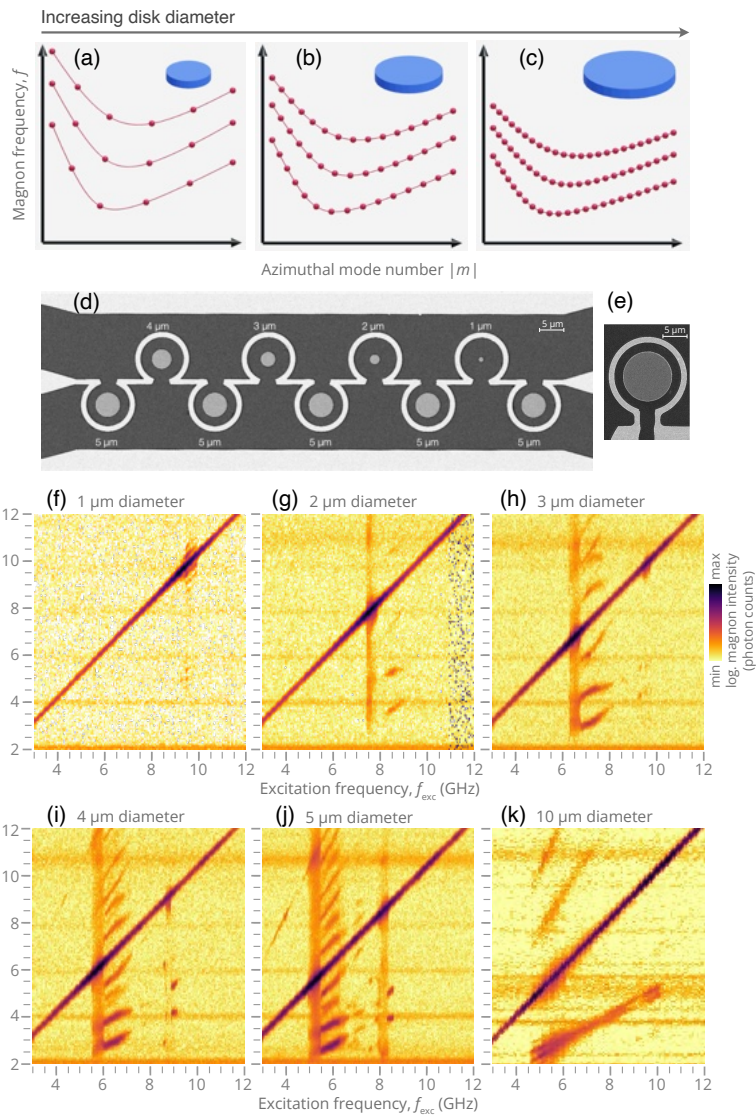


Figure 1: Dependence of the magnon eigenmode spectrum on the disk diameter. (a)-(c) The wider the disk, the denser are the modes in reciprocal space. (d),(e) Scanning electron micrographs of vortex-based magnon reservoirs with different diameters. (f)-(k) Magnon spectra measured as a function of the excitation frequency on disk-shaped reservoirs with different diameters. The differences in the nonlinear response directly reflects on the frequency range that is suitable for reservoir operation. In the 1 μm -wide disk (f), three-magnon splitting is hardly visible at an excitation frequency slightly below 10 GHz whereas in the 10 μm -wide disk (k), the range for nonlinear splitting is much larger.

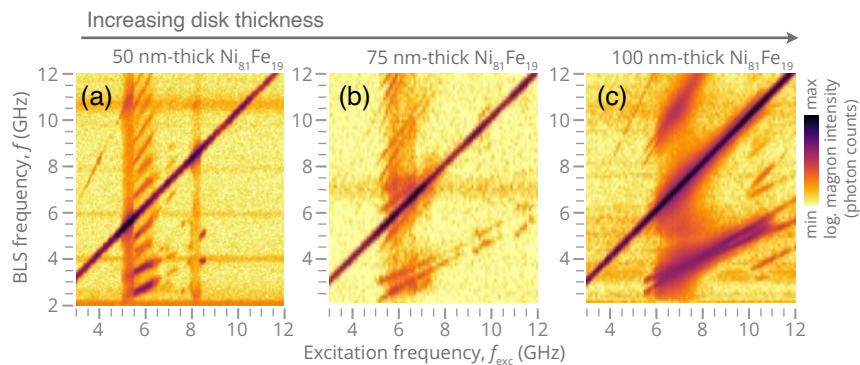


Figure 2: Dependence of the nonlinear magnon scattering on the disk thickness. Magnon spectra measured as a function of the excitation frequency on 5 μm -wide vortex-based $\text{Ni}_{81}\text{Fe}_{19}$ reservoirs with different thicknesses of (a) 50 nm, (b) 75 nm and (c) 100 nm.



75 nm, and 100 nm, respectively. One can see the general trend that thicker disks result in a larger range for nonlinear magnon scattering. While in the 50 nm-thick disk three-magnon splitting is only measured for excitation frequencies between 5 and 9 GHz, the range for nonlinear scattering extends to 12 GHz in the 100 nm-thick disk.

3. Vortex-based reservoirs with varying magnetic material

Another means to change the operating range for the magnon-scattering reservoir is by using a different magnetic material. The larger the saturation magnetization M_s , the steeper the initial drop of the magnon dispersion in the magnetic vortex-state disk. This leads to a broader range of excitation frequencies for which three-magnon splitting is possible. Figure 3 demonstrates this by comparing the nonlinear magnon response in (a) $\text{Ni}_{81}\text{Fe}_{19}$ and (b) $\text{Co}_{25}\text{Fe}_{75}$ which we measured using Brillouin light scattering microscopy, for each element integrating over several measurement positions to capture the different spatial mode profiles. The saturation magnetization of $\text{Co}_{25}\text{Fe}_{75}$ ($M_s = 1700$ kA/m) is slightly more than twice as large as the one of $\text{Ni}_{81}\text{Fe}_{19}$ ($M_s = 810$ kA/m). As a result, three magnon scattering in $\text{Co}_{25}\text{Fe}_{75}$ is observed for excitation frequencies from 7 to 17 GHz, whereas in $\text{Ni}_{81}\text{Fe}_{19}$ it is only measured between 5 and 9 GHz. Please note the different scales of the frequency axes.

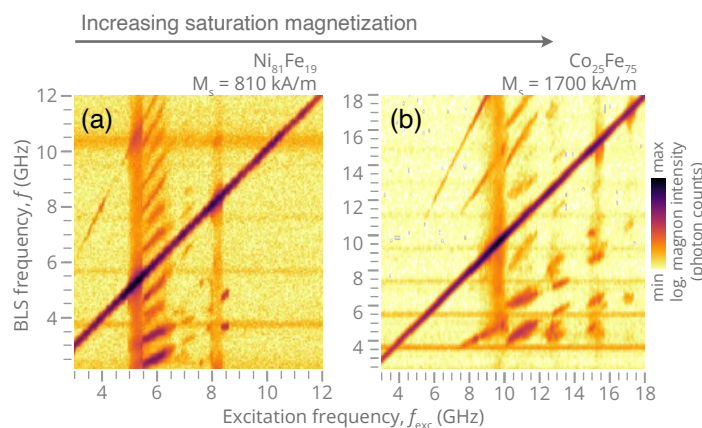


Figure 3: Three-magnon splitting in materials with different saturation magnetization. Magnon spectra measured as a function of the excitation frequency in vortex-based 5 μm -wide reservoirs fabricated from (a) $\text{Ni}_{81}\text{Fe}_{19}$ and (b) $\text{Co}_{25}\text{Fe}_{75}$.

4. Magnon reservoirs with different shapes

Besides magnetic vortices, a manifold of other two-dimensional magnon cavities can potentially serve as magnon reservoirs. Therefore, we designed ring-shaped microstructures using conventional electron-beam lithography, magnetron sputtering of the magnetic material and subsequent lift-off. As can be seen in the scanning electron microscopy images in Fig. 4a, the rings have the same outer diameter of 5 μm , only the central holes vary in diameter, which are given as labels above and below the rings, respectively. All rings are patterned from 50 nm-thick $\text{Ni}_{81}\text{Fe}_{19}$. Using Brillouin light scattering microscopy, we measured the nonlinear response on these different structures, for each element integrating over several measurement positions to capture the different spatial mode profiles. The BLS spectra are summarized for increasing hole diameter in Fig. 4b-i.



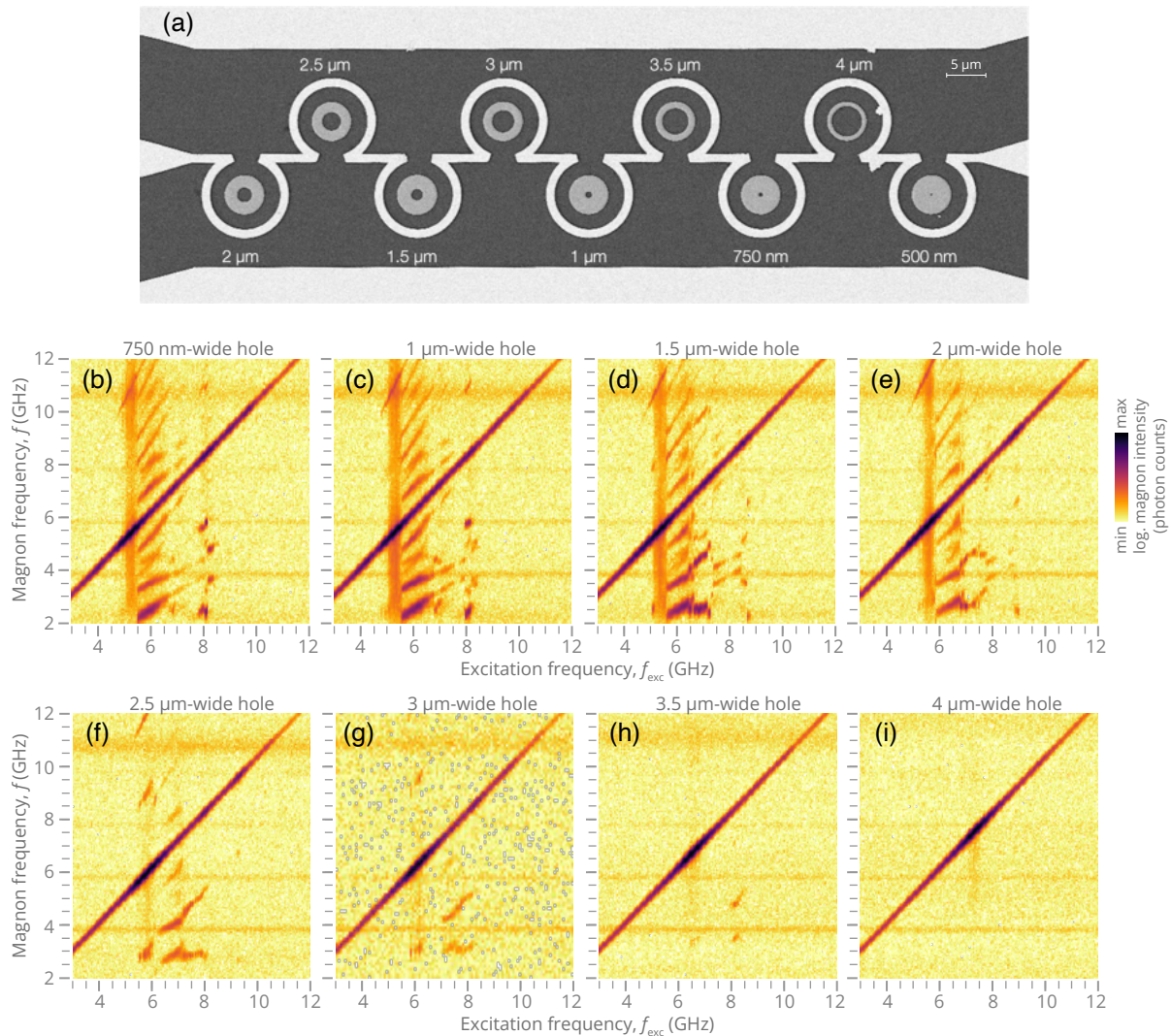


Figure 4: Three-magnon splitting in rings fabricated from 50 nm-thick $\text{Ni}_{81}\text{Fe}_{19}$. (a) Scanning-electron micrograph of different ring-shaped reservoirs, each positioned in an Ω -shaped microwave antenna. (b)–(i) Magnon spectra recorded as a function of the excitation frequency for different sizes of the ring's central hole. All rings have the same outer diameter of 5 μm . As can be seen by the off-diagonal signals, three-magnon splitting becomes less for larger hole diameters.

Due to the different quantization in radial direction, different channels for three-magnon splitting are accessible. While the rings with smaller holes show a large manifold of three-magnon splitting channels, the ring with a 4 μm -wide hole hardly shows any nonlinearity.

In addition to ring-shaped reservoirs, we fabricated ellipses with different aspect ratios and squares with different edge lengths. Figure 5a-d shows the scanning electron microscope images of the patterned ellipses which all have a 5.2 μm -long major axes but different aspect ratios of 2, 1.7, 1.4, and 1.2. Ellipses are specifically intriguing because of their magnetization configuration potentially changing for different aspect ratios. While ellipses with aspect ratios close to one will be more likely to form a single vortex state, large aspect ratios may lead to the formation of double vortex structures. In Fig. 5, the impact of these different magnetization configurations on nonlinear scattering may already be visible when comparing the BLS spectra recorded for the ellipse with an aspect ratio of 1.7 (Fig. 5f) to the other. For excitation frequencies between 6 and 8 GHz, three-magnon scattering is visible, however, not just following one channel but two. This means that four



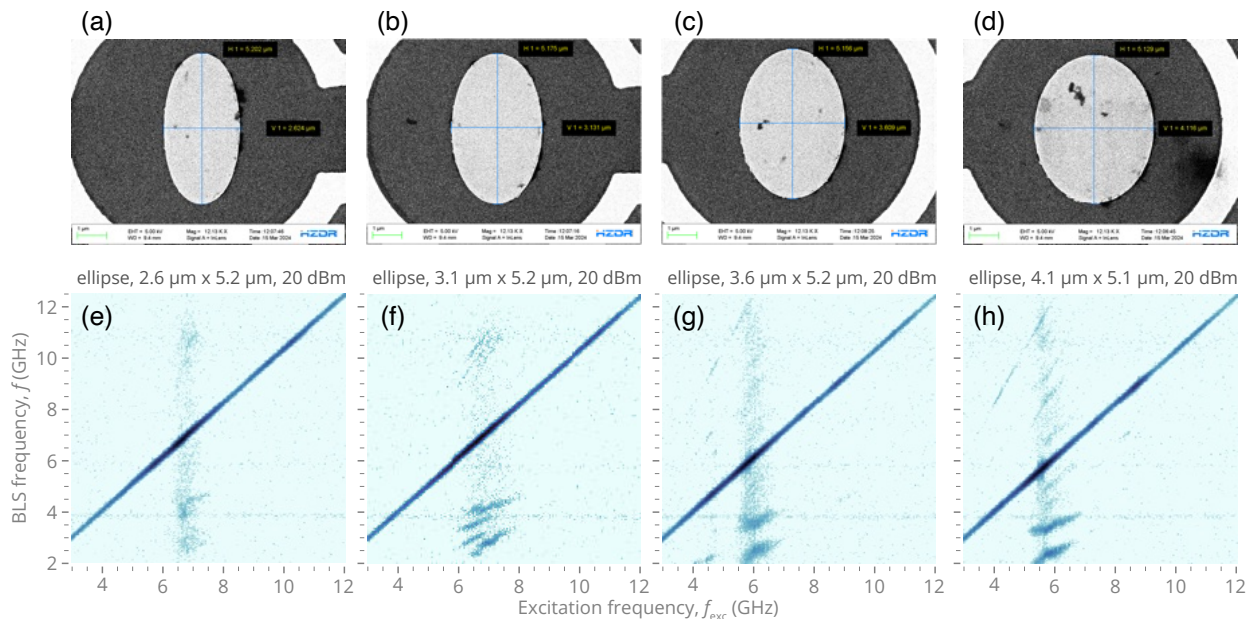


Figure 5: Three-magnon splitting in ellipses with different aspect ratios ranging from 2 down to 1.2. (a)-(d) Scanning electron microscope images of the ellipses fabricated from 50 nm-thick $\text{Ni}_{81}\text{Fe}_{19}$ positioned in an Ω -shaped antennas. (e)-(h) Magnon spectra recorded using Brillouin light scattering (BLS) microscopy as a function of the excitation frequency for ellipses with different aspect ratios. All ellipses share a common major axis of 5.2 μm . As can be seen by the off-diagonal signals, three-magnon splitting changes with the aspect ratio.

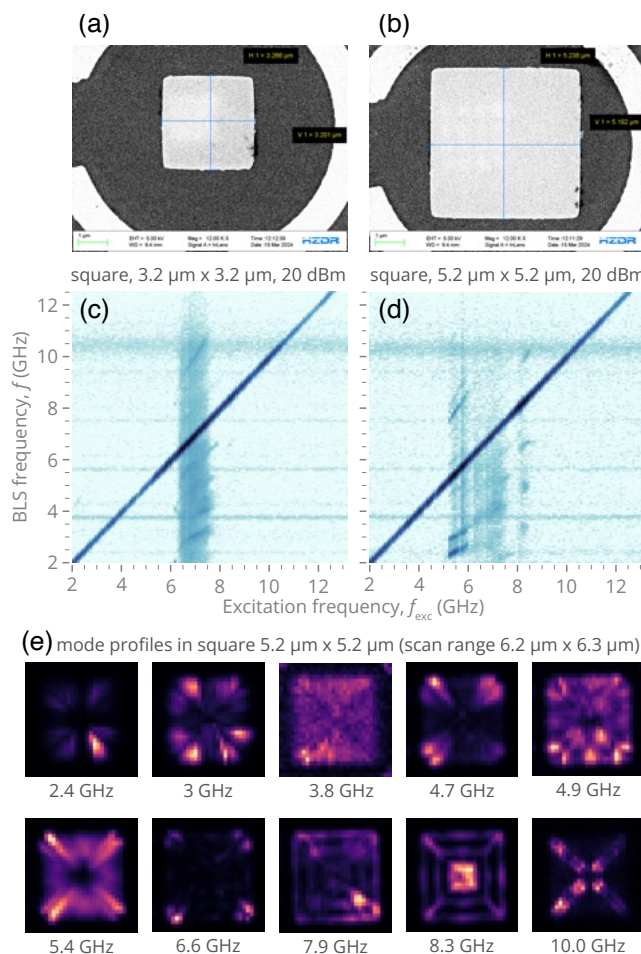


Figure 6: Three-magnon splitting in squares with different edge lengths. (a),(b) Scanning electron microscope images of the squares fabricated from 50 nm-thick $\text{Ni}_{81}\text{Fe}_{19}$ positioned in Ω -shaped antennas. (c)-(d) Magnon spectra recorded using Brillouin light scattering (BLS) microscopy as a function of the excitation frequency for squares with different edge lengths.



split modes are measured on the ellipse with an aspect ratio of 1.7 instead of two. This may be related to the different magnetic configuration of this specific ellipse, possibly exhibiting a double vortex. The other ellipses more closely follow the three-magnon splitting along one channel, as is known from disk-shaped reservoirs exhibiting a vortex state. Unfortunately, Brillouin light scattering microscopy does not allow for the simultaneous measurement of the magnetic ground state. Therefore, further studies are needed to determine the magnetic configuration in the ellipses with larger aspect ratios. Ultimately, the goal will be to design the magnetic configuration, both by shape and magnetic field cycling.

Figure 6a,b shows scanning electron microscope images of the studied square-shaped reservoirs with the corresponding BLS spectra plotted in Fig. 6c,d. As was already observed for the disk-shaped reservoirs with different diameter (Fig. 1), three-magnon splitting becomes more pronounced with increasing size of the squares. This is related to a denser mode packing in larger structures. Interestingly, the two-dimensional measurements of various mode profiles in the $5.2 \mu\text{m} \times 5.2 \mu\text{m}$ square in Fig. 6e suggest that their unique magnetization ground state of a Landau pattern with 90° domain walls offers a means for easier spatial separation of the different modes.

5. Conclusion

In general, the nonlinear scattering in most $\text{Ni}_{81}\text{Fe}_{19}$ reservoirs studied so far is in a similar frequency range between 5 and 10 GHz. Yet the exact nonlinear response is slightly different across all devices. This supports our hope to combine several reservoirs, feed them with the same input and obtain better results compared to addressing an individual reservoir alone. On the other hand, changing the magnetic material, e.g. $\text{Co}_{25}\text{Fe}_{75}$ instead of $\text{Ni}_{81}\text{Fe}_{19}$, sufficiently modifies the reservoirs' operating frequencies. Thereby, it should be possible to address elements made from different materials via individual inputs spanning separate frequency ranges. This would allow for parallel operation.

